Par3/Bazooka binds NICD and promotes Notch signalling during *Drosophila* development

Jun Wu, Neeta Bala Tannan, Linh T. Vuong, Yildiz Koca, Giovanna M. Collu, and Marek Mlodzik

Affiliations

Dept. of Cell, Developmental, and Regenerative Biology,

Graduate School of Biomedical Sciences,

Icahn School of Medicine at Mount Sinai,

One Gustave L. Levy Place, New York, NY 10029.

Abstract

The conserved *bazooka (baz/par3*) gene acts as a key regulator of asymmetrical cell divisions across the animal kingdom. Associated Par3/Baz-Par6-aPKC protein complexes are also well known for their role in the establishment of apical/basal cell polarity in epithelial cells. Here we define a novel, positive function of Baz/Par3 in the Notch pathway. Using *Drosophila* wing and eye development, we demonstrate that Baz is required for Notch signaling activity and optimal transcriptional activation of Notch target genes. Baz appears to act independently of aPKC in these contexts, as knockdown of *aPKC* does not cause *Notch* loss-of-function phenotypes. Using transgenic Notch constructs, our data positions Baz activity downstream of activating Notch cleavage steps and upstream of Su(H)/CSL transcription factor complex activity on Notch target genes. We demonstrate a biochemical interaction between NICD and Baz, suggesting that Baz is required for NICD activity before NICD binds to Su(H). Taken together, our data define a novel role of the polarity protein Baz/Par3, as a positive and direct regulator of Notch signaling through its interaction with NICD.

Key Words:

Notch signaling, Par3, transcriptional target regulation, cell polarity, Drosophila, tissue patterning

Introduction

Cell polarity is a critical feature of most cell types, particularly epithelial cell sheets, which display obligate apical-basal (A/B) polarity that is required for their barrier function and vectorial secretion. Many proteins and mechanisms that govern the establishment and maintenance of cell polarity are evolutionarily conserved and were discovered genetically in *C. elegans* and *Drosophila* (reviewed in (Goldstein and Macara, 2007; St Johnston and Sanson, 2011; Tepass, 2012)). Similarly, stem cells often display polarized features using the same factors, which are critical for stem cell maintenance and for progenitor cell fates, with cell contents being asymmetrically inherited by the two daughter cells (e.g. rev. in (Neumuller and Knoblich, 2009; Schweisguth, 2015)). The protein complexes that mediate polarization are also shared among these distinct instances of cell polarization.

The conserved *par3* gene, known as *bazooka/baz* in *Drosophila*, was originally identified in *C. elegans*, where it acts as a key regulator of asymmetrical cell divisions in the early embryo (Etemad-Moghadam et al., 1995). It generally acts together with Par6 and aPKC as a regulatory complex of many asymmetric cell divisions across the animal kingdom (reviewed in (Neumuller and Knoblich, 2009; Schweisguth, 2015)). This Par3/Baz-Par6-aPKC complex is also well known for its conserved role in the establishment of A/B polarity in epithelial cells (Suzuki and Ohno, 2006). Our interest in the A/B epithelial cell polarity proteins originates from the fact that several of these have also been linked to planar cell polarity (PCP), that is polarity within the epithelial sheet, orthogonal to the A/B axis (Humphries and Mlodzik, 2018). For example aPKC can associate with Frizzled, and Scribble (another A/B polarity protein) associates with the PCP protein Van Gogh/Vang (Vangl in vertebrates) (Courbard et al., 2009; Djiane et al., 2005). aPKC and Scribble thus contribute to the stability and asymmetric segregation of the core PCP complexes and establishment of planar polarity within epithelial cell sheets. To systematically examine whether additional A/B epithelial polarity factors can play a role in PCP establishment,

we tested members of these protein families for PCP associated knockdown phenotypes during *Drosophila* wing development. Surprisingly when we examined phenotypes of *baz/par3* knockdown in this context, we observed a *Notch* mutant-like phenotype of loss of wing margin tissue. Here we focus on investigating a specific role for Baz in regulating Notch signaling.

Notch (N) was originally identified in *Drosophila* based on its haplo-insufficient, dominant wing-notching phenotype of loss of tissue at the dorso-ventral border of the wing (Guruharsha et al., 2012; Mohr, 1919; Southgate et al., 2015). *Notch* encodes a single-pass transmembrane receptor protein containing EGF-like repeats in its extracellular domain (Wharton et al., 1985) and a conserved intracellular domain (NICD) that, upon cleavage, can translocate to the nucleus and function as transcriptional co-activator (reviewed in (Andersson et al., 2011; Bray, 2016; Henrique and Schweisguth, 2019; Kopan and Ilagan, 2009; Wilson and Radtke, 2006)). Many studies demonstrated that the highly conserved Notch receptor family plays important roles during the development and homeostasis of most tissues through cell-cell communication and cellular signaling, controlling many target genes that can be either common or context dependent (reviewed in (Andersson et al., 2011; Bray, 2016; Henrique and Schweisguth, 2019; Kopan and Ilagan, 2009; Wilson and Radtke, 2006) (Siebel and Lendahl, 2017)). Misregulation of N-signaling is associated with many human diseases, including cancer (Siebel and Lendahl, 2017). The Notch receptor is activated by the binding of ligands of the Delta (Dl) or Serrate/Jagged (Ser) families from neighboring cells to trigger juxtamebrane cleavage events to release NICD (Andersson et al., 2011; Bray, 2016; Struhl and Greenwald, 1999). NICD can then translocate into the nucleus, where it interacts with transcription factors of the Suppressor of Hairless (Su(H)/CSL) family, and co-activators, including Mastermind, to activate target gene expression (Bray, 2016). Notch signaling is subject to many regulatory steps that have been and continue to be identified and characterized in *Drosophila*, ranging from receptor and ligand trafficking, receptor glycosylation, membrane lipid composition, receptor cleavage, and protein

stability regulators (Bala Tannan et al., 2018; Kandachar and Roegiers, 2012; Kidd et al., 1998; Medina-Yáñez et al., 2020; Rana and Haltiwanger, 2011; Shilo and Schejter, 2011; Singh and Mlodzik, 2012; Struhl and Greenwald, 1999; Weber et al., 2003) to specific nuclear events at the transcriptional end of pathway activation (rev. in (Andersson et al., 2011; Bray, 2016; Henrique and Schweisguth, 2019; Kopan and Ilagan, 2009; Wilson and Radtke, 2006)).

Previous work proposed an indirect role for Baz/Par3 in regulating Notch signaling during asymmetric cell divisions in *Drosophila*. During asymmetric cell division of the sensory organ precursors (SOPs), specific protein complexes segregate to opposite sides of the cell cortex in each dividing SOP cell, on one side the Baz/Par3-Par6-aPKC complex and on the other the Gai-Pins-Mud-Dlg-Numb-Neur complex. The two daughter cells that result from this cell division adopt distinct cell fates due to the asymmetric distribution of the above complexes: with one daughter cell inheriting Baz/Par3-Par6-aPKC, and the other the Gai-Pins-Mud-Dlg-Numb-Neur complex (Schweisguth, 2015). Notably, the asymmetric segregation of these complexes causes an asymmetric activation of Notch signaling, as Numb is known to repress N-signaling by reducing Notch levels at the cell surface, either through internalization or inhibition of recycling (Schweisguth, 2015). In a similar scenario, in the context of intestinal stem cell (ISC) number regulation, Baz is also required within the asymmetric apical-basal polarity complex segregation to regulate Notch activity (Wu et al., 2023). As such, an indirect role of Baz/Par3 in the regulation of N-signaling has been proposed, acting through the promotion of the asymmetric segregation of the respective apical-basal complexes to allow Notch activity in the Baz-containing daughter cells. However, due to this indirect role of Baz/Par3 in the pathway, such model systems are not suited to address potential direct roles of Baz/Par3 in Notch-signaling.

Using *Drosophila* wing and eye development, we define a novel, direct and positive function of Baz/Par3 in Notch signaling. We demonstrate that Baz is required for Notch signaling activity

118 and activation of Notch transcriptional target genes. Baz appears to act independently of aPKC
119 in these contexts, as knockdown of *aPKC* causes PCP defects and not Notch-associated
120 phenotypes. Our data indicate that Baz acts the level of NICD, the cleaved active Notch
121 fragment, but upstream of the Su(H)-NICD-Mam activation complex. We further demonstrate a
122 direct biochemical interaction between NICD and Baz. Taken together, our data define a novel
123 role of the polarity protein Baz/Par3, as a positive regulator of Notch signaling through its
124 interaction with NICD.
125
126 **Results**
127 **Reduction of *baz/par3* causes defects similar to *Notch* loss-of-function phenotypes**
128 To initially assess potential functions of Baz/Par3-Par6-aPKC factors in PCP we expressed two
129 independent non-overlapping RNAi (IR) lines for each gene in the posterior compartment of
130 developing wing discs using the *en-Gal4* driver (Figure 1 and Suppl. Figure S1). Surprisingly,
131 with individual components of the A/B polarity complex containing Baz/Par3, Par6, and aPKC
132 we detected distinct outcomes. While knock-down of aPKC showed classical PCP defects, as
133 expected based on previous work (Djiane et al., 2005) (see also below), both *baz-IR* lines
134 caused wing margin loss in the posterior compartment (Figure 1A-C; Baz protein levels were
135 markedly reduced and barely detectable in the *baz-IR* expressing domain: Figure 1E, and
136 Suppl. Figure S1B-C). The loss of the wing margin is associated with a reduction in Notch
137 signaling or in effects on the Wg signaling pathway, as *wg* is a direct target of Notch signaling
138 along the dorsal/ventral compartment border. Besides the posterior compartment of the wing
139 being slightly reduced, no other patterning defects were observed in the *baz* knockdowns
140 (Figure 1A-C). In contrast to *baz*, knockdown of either *aPKC* or *par6* caused cell lethality with
141 loss of large areas of the posterior wing compartment at 25°C or 29°C (Suppl. Figure S1). When
142 *aPKC-IR* was expressed at reduced levels (driven at 18°C), causing a milder knock-down, the
143 posterior wing compartment was still markedly smaller (Figure 1D; note that wing hairs were

144 also often very short, Fig. 1D-D', orange arrows), but the wing margin appeared largely normal
145 (Figure 1B'-D'). PCP defects were also observed in the *aPKC-IR* expressing domain (Figure
146 1D', green arrow indicating PCP hair orientation), consistent with the previously identified role of
147 aPKC in PCP (Djiane et al., 2005). *Par6-IR* mediated knock-down caused severe loss of wing
148 tissues even at 18°C, making it impossible to correlate these defects with a specific cellular
149 mechanism or signaling pathway (Suppl. Figure S1D-D'). Nevertheless, the wing margin
150 appeared relatively normal in areas where there was no tissue loss (Suppl. Figure S1D-D',
151 magenta arrows).
152
153 Taken together, knockdown of *baz* caused a distinct loss-of-function (LOF) phenotype from
154 *aPKC* and *Par6*, affecting wing margin development. To confirm this effect, we also analyzed
155 wings containing mutant clones of baz^{4} or $baz^{815\text{-}8}$ alleles (Suppl. Figure S1A for allele
156 information). Consistent with the RNAi knock-downs, *baz* LOF clones also displayed wing
157 margin loss (Suppl. Figure S2A-C). On the notum, *baz* mutant LOF clones displayed loss of
158 sensory bristles (Suppl. Figure S2D-F), in accordance with previous work (Roegiers et al., 2001)
159 confirming the behavior of the *baz* alleles. Taken together with the RNAi phenotypes above, the
160 *baz* LOF clonal phenotypes in the wing suggest a potential role for Baz/Par3 in Notch-signaling.
161
162 ***Notch* and *baz* interact genetically**
163 To corroborate a relationship between *Notch* and *baz* phenotypes, we performed genetic
164 interaction analyses. In heterozygous conditions of the null allele N^{55e11}/+, approx. 30% of wings
165 displayed distal margin notching (near vein 3 and 4; Figure 2A, B, and F). We compared these
166 wings to double heterozygous combinations with the LOF *baz* alleles: baz^{4} or $baz^{815\text{-}8}$.
167 Strikingly, the double heterozygous animals displayed a marked enhancement of wing notching
168 with 68% and 79% of wing margin defects in N^{55e11}/baz^{4} and $N^{55e11}/baz^{815\text{-}8}$ allelic combinations,
169 respectively (Figure 2C-D, and F; see also Suppl. Figure S3). Moreover, in addition to the

170 enhanced distal wing notch phenotype, a novel defect appeared in the double heterozygous
171 animals with wing notching in the proximal region of the posterior compartment (Figure 2B', D'
172 and quantified in 2G; see also Suppl. Figure S3B'-C'). Whereas N^{55e11}/+ wings did not display
173 any margin defects in this proximal region (Figure 2B' and 2G), 100% of the double
174 heterozygous N^{55e11}/baz^{4} and $N^{55e11}/baz^{815\text{-}8}$ wings carried such margin defects (quantified in
175 Figure 2G; $p<0.0001$). The equivalent baz^{4}/+ and $baz^{815\text{-}6}$/+ heterozygous control wings did not
176 display any margin notching phenotypes (Figure 2E-E', also Suppl. Figure S3C-C'). These data
177 suggest that *Notch* and *baz* genetically interact during wing margin patterning in a synergistic
178 manner.
179
180 We next asked whether interactions between *Notch* and *baz* are also detected in other tissues
181 and with a gain-of-function (GOF) N genotype. The specification of cell fates in the developing
182 eye requires Notch input at multiple steps, from early patterning of the presumptive eye field to
183 the specification of individual photoreceptor (R cell) and accessory cell fates. A classical assay
184 for N-signaling during eye patterning is the expression of constitutively active (ca)-N molecules
185 under control of the *sevenless* (*sev*) enhancer (expressed in R3-4 and R1,6, and R7). Such ca-
186 Notch molecules are either N-terminally truncated molecules that lack the inhibitory region in the
187 extracellular domain preventing g-secretase-mediated cleavage (NDECD, (Fortini et al., 1993)),
188 or the intracellular domain itself, which lacks the membrane targeting sequence (NICD, (Kidd et
189 al., 1998)). Depending upon the strength of activation, ectopic Notch activity induces the
190 transformation of R3 to R4 and/or the R1/R6 photoreceptors to R7 (Cooper and Bray, 1999;
191 Fanto and Mlodzik, 1999; Tomlinson and Struhl, 1999, 2001). The induction of R7 is a classical
192 Notch-dependent cell fate and ectopic activation of N causes the transformation of R1/R6
193 photoreceptors to R7 independently of any PCP input (Tomlinson and Struhl, 2001). In the *sev-*
194 *NICD* background a large fraction of ommatidia display a multi-R7 phenotype (Figure 2H, and
195 (Tomlinson and Struhl, 2001)), while the presence of one copy of the strong $baz^{815\text{-}8}$ allele in this

196 background suppresses the GOF Notch effect (Figure 2H). Taken together with the above
197 genetic interactions with *N* LOF features, these results suggest that Baz/Par3 is generally
198 required for Notch signaling function in different tissues and contexts, as seen in both, LOF and
199 GOF, scenarios.
200
201 ***baz* loss-of-function leads to reduction of Notch target gene expression**
202 To test whether *baz-IR* affects Notch signaling directly, we examined the expression of the
203 endogenous Notch signaling targets *wg* and *cut* (Micchelli et al., 1997; Neumann and Cohen,
204 1996). To monitor *wg* expression we analyzed the expression of *wg-lacZ*, an enhancer trap
205 insertion in the *wg* locus, which faithfully reproduces *wg* expression patterns (Kassis et al.,
206 1992); and to monitor *cut* expression we used an antibody to Cut. Knock-down of *baz* in the
207 posterior compartment caused reduction of both *wg-lacZ* expression and Cut protein levels, as
208 compared to control levels in the anterior compartment (Figure 3A-C"). Both *wg-lacZ* and Cut
209 levels were significantly reduced in quantifications of their intensity ratio between the anterior
210 (control) and posterior (experimental) compartment (Figure 3D-E). Since the reduction of *wg*
211 and *cut* expression is detected at the third instar larval stage in wing discs, before sensory
212 development occurs at the pupal stages (Jack et al., 1991), the *baz* effect on their expression
213 precedes sensory cell differentiation and is thus clearly separated in time from the known Baz
214 function in asymmetric SOP cell division.
215
216 To confirm these results, we also examined the expression of a synthetic reporter containing the
217 Notch response element (NRE), *NRE-GFP* (Furriols and Bray, 2001; Saj et al., 2010). In wing
218 discs, *NRE-GFP* is expressed along the dorsal/ventral compartment border in pattern
219 indistinguishable from endogenous Notch target genes such as *wg* and *cut* (Saj et al., 2010)
220 (Suppl. Figure S4A). Importantly, reduced expression of *NRE-GFP* was observed in the

221 posterior compartment in *enGal4>baz-IR(s)* wings (Suppl. Figure S4B-C', and E), indicating that
222 a reduction of *baz* directly correlated with reduced Notch-signaling and target gene expression.
223
224 To corroborate these data and to test for a general effect of *baz* LOF on Notch signaling
225 outcomes in different experimental set ups, we analyzed the expression of Notch targets in *baz*
226 mutant clones. Consistent with the *baz-IR* knockdown in wing discs, Cut expression levels were
227 reduced in $baz^{815\text{-}8}$ mutant cells (clones were positively labeled by RFP expression, Figure 4A-C,
228 examples highlighted with white arrows; quantified in Figure 4D). Next we tested for effects on
229 Notch signaling in eye discs. To test an independent Notch target gene, we asked whether
230 expression of *atonal* (*ato*), a N-signaling target during early eye patterning prior to R-cell
231 specification (Freeman, 2001) also requires *baz* for its full expression. Ato levels were reduced
232 in $baz^{815\text{-}8}$ mutant cells (orange arrows in Figure 4E-E", F-F", mutant clone marked by lack of
233 GFP). Importantly, apical-basal polarity as apparent in optical z-sections was normal in baz^{-}
234 clones (Figure 4G-G"; note Patj as A/B marker being localized normally in $baz^{815\text{-}8}$ clones – see
235 Discussion), whereas a reduction of Ato expression was also easily detected in this optical
236 plane (Figure 4D-F, orange arrows in E" and F"; quantified in Figure 4H),
237
238 Taken together, these results are consistent with the notion that Baz functions as a positive
239 regulator within the Notch-signaling pathway, promoting the expression of Notch target genes.
240
241 **Baz affects Notch-signaling at the NICD level**
242 To mechanistically dissect Baz function in Notch signaling, we used N-terminal Notch
243 truncations in GOF assays to determine at what level within the pathway Baz was required.
244 First, we used NDECD (Fortini et al., 1993), which lacks the extracellular domain and is
245 constitutively active independent of ligand binding (see above). As such, if NDECD were
246 affected by *baz* LOF, Baz would be required downstream of the N-ligands and the subsequent

247 extracellular cleavages of Notch, but upstream of the g-secretase-mediated cleavage
248 (Andersson et al., 2011; Struhl and Greenwald, 1999). When NDECD was clonally expressed in
249 larval wing discs, 43% of NDECD clones induced the Notch target *wg* (Figure 5A, F; as detected
250 by Wg antibody). When *baz-IR(*s) were co-expressed with NDECD, the frequency of clones
251 expressing Wg was reduced to 20% (*baz-IR*-1) and 27% (*baz-IR*-2), respectively (Figure 5B, F).
252 These data suggested that Baz was required at the level of the g-secretase cleavage or further
253 downstream within the Notch-signaling pathway. Consistent with this hypothesis *baz-IR* knock-
254 down displayed no detectable effect on Notch protein levels at the membrane or cellular
255 distribution of Notch (Suppl. Figure S1E-F).
256
257 To further investigate the position of Baz within the Notch pathway, we tested the NICD
258 fragment, which is fully active and does not associate with the membrane or require any
259 cleavage and is thought to directly translocate to the nucleus to activate Notch-signaling target
260 genes as transcriptional co-activator (Andersson et al., 2011; Bray, 2016; Struhl and Greenwald,
261 1999). In control wing disc clones expressing NICD, Wg expression was readily detected in 63%
262 of clones (or 71% with a control IR co-expression) (Figure 5C-D, and G). In experimental
263 clones, with *baz-IR*(s) being co-expressed with NICD, the NICD effect was markedly
264 suppressed: to 41% with *baz-IR*-1 and 32% with *baz-IR*-2, respectively (Figure 5E, G). These
265 data are consistent with the notion that Baz acts downstream of membrane tethered Notch and
266 that it is required for the NICD fragment to activate Notch-signaling target gene expression.
267
268 In the nucleus, NICD functions as a co-activator interacting with Su(H) (the *Drosophila* member
269 of the CSL transcription factor family), Mastermind (Mam), and other co-activators to form a
270 complex (or complexes) at transcriptional enhancer sites to activate Notch target gene
271 expression (Bray, 2016). To gain insight into whether Baz/Par3 promotes the formation of the
272 Su(H)-NICD-Mam complex, we asked *whether baz* LOF could reduce the activity of an active

273 Su(H)-Ank fusion protein. A direct fusion of the Ankyrin repeats of Notch to Su(H), was shown in
274 *Xenopus* to bypass a requirement for endogenous Notch itself by directly recruiting Mam, and
275 thus it is acting even further "downstream" relative to NICD in the pathway (Wettstein et al.,
276 1997). To this end, we generated a *Drosophila* version of the construct, fusing the Notch ankyrin
277 repeat region to the Su(H) protein [yielding Su(H)-Ank]. We used the clonal expression assay in
278 the wing pouch, as used above for NICD for example (Figure 5), and expressed Su(H)-Ank in
279 equivalent clones with *baz-RNAi*. Strikingly, clonal expression of Su(H)-Ank alone or together
280 with *baz-RNAi* showed similar percentages of clones inducing expression of *wg* (Suppl. Figure
281 S5). This result demonstrates that Su(H)-Ank activates Notch target gene expression
282 independently of Baz. Taken together with the clonal behavior of NICD, these data suggested
283 that Baz acted on NICD, upstream of the Su(H) based transcription complex, prior to NICD
284 association with Su(H) and Mam (see Discussion).
285
286 To complelement the above *in vivo* studies we next addressed whether Baz and NICD could
287 physically interact. This was tested biochemically via co-immunoprecipitation (co-IP) in S2 cells
288 that were co-transfected with HA-tagged NICD and either Baz-myc (full length Baz tagged with
289 myc) or myc-Hippo (Hpo, as negative control). Protein extracts were immunoprecipitated with
290 anti-myc antibody and analyzed by immunoblotting with anti-HA antibody. NICD was readily co-
291 immunoprecipitated with Baz-myc (Figure 6A), but not by the Hpo negative control (Figure 6A-B;
292 see figure legend for additional controls), suggesting that NICD and Baz/Par3 can physically
293 associate.
294
295 Taken together with the functional *in vivo* data, these results suggested that Baz and NICD were
296 associated in the same protein complex, and that the presence of Baz is required for normal
297 NICD function in Notch target gene induction. However, Baz appeared to act upstream of the

298 Su(H) based transcription factor complex, as it did not have an effect in the context of the
299 Su(H)-Ank fusion, which bypassed a requirement for NICD.
300
301 **Baz and Numb are required at different levels within the Notch pathway**
302 To gain further mechanistic insight into how Baz might affect NICD, we tested the relationship of
303 Baz to Numb, which has itself a complex relationship to Notch-signaling (see also Introduction).
304 While Numb has been shown to regulate Notch-signaling at the level of trafficking of the
305 receptor (Couturier et al., 2013; Houssin et al., 2021; Schweisguth, 2015), it has also been
306 reported to directly interact with NICD and inhibit Notch signaling at the NICD level (Frise et al.,
307 1996; Guo et al., 1996). To address these possibilities, we wished to test whether *numb* and
308 *baz* could interact genetically with each other in the above wing margin specification context.
309 First we asked, whether reduction of *baz* function (via *baz-RNAi* equivalent to experiments
310 shown in Figure 1) could be modified by Numb levels. Indeed, loss of wing margin bristle cells
311 (Figure 7A, C, D, F) was suppressed upon removal of one *numb* gene copy, in a $numb^{15}$/+
312 heterozygous background (Figure 7B, C, E, F), displaying a dosage sensitive relationship
313 between the two proteins. To confirm this, we compared phenotypes induced by overexpression
314 of *numb-GFP* with or without *baz-Flag* in developing wings. Overexpression of *numb-GFP*
315 suppressed Notch signaling, as detected by margin bristle loss (Suppl. Figure S6A-B and D,
316 (Frise et al., 1996); of note, Numb-GFP also inhibited Notch function in the context of wing vein
317 formation). Co-overexpression of *baz-Flag* with *numb-GFP* reduced the inhibitory effect of
318 Numb on Notch signaling at the wing margin (Suppl. Figure S6B-D). These experiments support
319 the notion that *numb* and *baz* antagonize each other genetically during wing margin cell
320 induction with Baz promoting Notch function and Numb inhibiting it.
321
322 We next wished to test whether they could act at the same level in Notch-signaling, at the level
323 of NICD. To this end, we asked whether the NICD clonal expression phenotype, induction of

324 target gene expression, which is suppressed by *baz-IR* (see Figure 5 in Results above), could
325 also be affected by Numb levels. Again, clonal NICD expression in the wing pouch induced
326 Notch-signaling target genes, for example *wg* (Figure 5) and *cut* (Figure 7G-G') and the removal
327 of *baz* (via RNAi) in such clones reduced the ability of NICD to induce target gene expression
328 (see Figure 5E,G). We thus asked whether co-overexpression of *numb-GFP* in such NICD
329 expression clones could also suppress NICD's function in target gene activation. However, we
330 did not observe an effect of Numb-GFP overexpression on NICD function in target gene
331 expression (Figure 7G-H, quantified in 7I, as shown for Cut). Taken together with the genetic
332 interactions above, these data suggested that Numb and Baz act at different levels in the Notch
333 pathway, with Numb acting further upstream and Baz/Par3 acting at the level of NICD.
334
335
336 **Discussion**
337 In this study we define a novel, direct, and positive role of the polarity protein Baz/Par3 in the
338 Notch pathway. This stands in contrast to its previously established role in Notch signaling
339 regulation during asymmetric SOP cell divisions, where Baz/Par3 affects N-signaling indirectly
340 by asymmetrically preventing the inheritance of the Notch inhibitor Numb (Schweisguth, 2015).
341 In the SOP scenario, the Baz/Par3-Par6-aPKC protein complex localizes to one side within the
342 dividing cell, and a Numb-Neuralized containing complex localizes to the other side of the cell.
343 As Numb inhibits Notch signaling by regulating Notch-Sanpodo trafficking and thus reducing
344 Notch levels at the cell surface, this asymmetry causes Notch inhibition in the Numb containing
345 daughter cell (reviewed in (Schweisguth, 2015)). In the SOP context, Baz/Par3 has been thus
346 proposed to have a passive role in N-signaling activation, via inhibiting an inhibitor, Numb. Our
347 data are consistent with the notion that Baz/Par3 is also required positively for the Notch
348 signaling response and full transcriptional activation of Notch targets in *Drosophila* in multiple
349 cell types. Genetic epistasis studies indicate that Baz acts at the level of cleaved active Notch,

350 NICD, or in parallel to it. Consistent with this notion Baz and NICD co-immunoprecipitated,
351 suggesting that Baz promotes Notch signaling at the level of NICD.
352
353 **A novel Baz/Par3 function independent of the A/B polarity complex**
354 Baz/Par3 is generally associated with Par6-aPKC at early to intermediate stages of A/B polarity
355 establishment, but later in mature epithelia it is no longer essential for their maintenance
356 (Morais-de-Sa et al., 2010; St Johnston and Sanson, 2011; Tepass, 2012). Indeed, the fact that
357 we can recover *baz* LOF clones at all, whereas Par6 and aPKC null alleles are cell lethal,
358 suggests that *baz* can behave differently to the 'core' A/B factors. In our experimental set-up we
359 observed no evidence for a Par6 or aPKC involvement in Notch signaling. Our data suggest that
360 Baz/Par3 regulates NICD independently of its role in the A/B polarity complex. Similar to A/B
361 polarity establishment, in the context of planar cell polarity (PCP) patterning, Baz/Par3 functions
362 together with aPKC to regulate Frizzled levels (and hence the PCP outcomes) in the *Drosophila*
363 eye (Djiane et al., 2005), and thus, while Par6 could not be assayed in this context, these data
364 suggested that in PCP determination Baz is functioning with established A/B polarity factors. As
365 such, the discovery that in Notch signaling Baz/Par3 appears to function independently of its
366 partners in A/B establishment within the same tissue is unexpected.
367
368 Par3 homologues have however been shown to act independently of the aPKC-Par6 complex in
369 several scenarios in mammalian cells, including Hippo/Yap signaling and during epithelial-
370 mesenchymal transition (Zhang et al., 2016). Par3 has even been suggested to act with Ku70
371 and Ku80 as part of the DNA-dependent protein kinase complex to regulate double-strand
372 breaks (Fang et al., 2007).
373
374 **Why was Baz/Par3 not identified earlier as a component of Notch signaling?**

375 The Notch pathway genes were initially identified through classic genetic collections of
376 spontaneous mutants showing morphological defects in *Drosophila* and *C. elegans* (Fleming et
377 al., 1990; Greenwald, 1985; Kopczynski et al., 1988; Lindsley and Zimm, 1992). Subsequent
378 genetic screens and molecular studies have added many components of the Notch pathway
379 and many regulatory mechanisms that affect Notch signaling at all levels, ranging from receptor
380 and ligand trafficking and membrane stability and its membrane associated proteolytic
381 cleavages to nuclear co-factors and chromatin associated target gene regulation (reviewed in
382 (Bray, 2016; Henrique and Schweisguth, 2019; Kopan and Ilagan, 2009). In particular, many of
383 the screens were performed using the notum Notch associated phenotypes and score for
384 asymmetric division-dependent SOP/bristle patterning defects. It has thus been technically
385 difficult, if not impossible, to separate potential additional Baz/Par3 involvements in Notch
386 signaling. Similarly, classical loss-of-function screens in the *Drosophila* embryo would have
387 missed Baz/Par3 due to its initial requirement in epithelial polarization that could have caused
388 earlier lethality (Harris and Peifer, 2004; Muller and Wieschaus, 1996), which obscures a
389 potential role in subsequent signaling events. Indirectly through our screen asking whether A/B
390 polarity factors can also play a role in PCP establishment in the posterior wing disc
391 compartment we used a unique experimental scenario: first the margin loss is due to tissue loss
392 and not asymmetric division of innervated SOPs, and, second, at this later stage of the epithelial
393 sheet is fully formed and Baz/Par3 is not required for maintenance of A/B polarity. This
394 combination thus allowed the identification of *baz* as a novel factor that positively regulates
395 Notch signaling in general.
396
397 **Baz/Par3 has multiple independent functions during Notch signaling.**
398 Baz/Par3 and Numb have both been implicated in the regulation of Notch signaling via
399 trafficking of the Notch receptor (Couturier et al., 2013; Houssin et al., 2021; Schweisguth,
400 2015). In addition, independent of trafficking, Numb has been suggested to inhibit Notch

401 signaling directly by binding to NICD (Frise et al., 1996; Guo et al., 1996). Overexpression of
402 Numb indeed can interfere with Notch signaling at the wing margin, causing significant Notch
403 loss-of-function type defects ((Frise et al., 1996) and this work). To address this directly, we
404 asked whether Numb overexpression could interfere with NICD function in the context Notch
405 target gene activation. However, NICD activity was not affected by Numb overexpression,
406 suggesting that it acted further upstream, likely as suggested at the level of regulating Notch
407 trafficking, which is consistent with previous studies (Couturier et al., 2013; Houssin et al.,
408 2021). In contrast to *numb*, knockdown of *baz/par3* directly affected NICD function and
409 reduction of Baz/Par3 levels significantly reduced NICD function in target gene activation.
410 Therefore, Baz/Par3 can act at two independent levels within Notch signaling, affecting (i)
411 membrane trafficking of the Notch receptor (Couturier et al., 2013; Houssin et al., 2021;
412 Schweisguth, 2015) and (ii) serving a positive function downstream in the pathway at the NICD
413 level (see below).
414
415 **Baz acts at the NICD level affecting expression of N-signaling targets positively**
416 The Notch-signaling associated DNA binding complex is centered around the Notch-pathway
417 dedicated DNA-binding factor CSL, Su(H) in *Drosophila*, and it switches from a repressor
418 complex to a transcriptional activator complex via NICD (Bray, 2016). NICD binds to Su(H), and
419 recruits co-activators including Mastermind (Mam), and its binding to Su(H)/CSL displaces the
420 "repressor complex" and induces N-signaling target gene transcription. Several factors have
421 been identified that associate with Su(H)/CSL and NICD (see reviews (Borggrefe and Oswald,
422 2009; Bray, 2016)). Genetic epistasis data, both in the wing and the eye, position the function of
423 Baz/Par3 at the level of NICD after its last cleavage, suggesting that Baz might act in the
424 nucleus together with NICD or alternatively it might promote stability, nuclear translocation,
425 function, or retention of NICD. The biochemical immunoprecipitation results support the genetic
426 data and are consistent with the notion that Baz is a direct regulator of Notch signaling, acting at

427 the level of NICD. However, the Su(H)-Ank fusion appears to not require Baz/Par3 for its
428 capability to activate Notch target gene expression, with *baz* knockdown having no effect on
429 Su(H)-Ank mediated activation, unlike with NICD, suggesting that Baz is acting upstream of the
430 Su(H)-Ank association. The Ank repeats of NICD are critical within the Notch protein for its
431 nuclear response as part of the Su(H) transcription factor complex by recruiting Mastermind,
432 and as such a Su(H)-Ank fusion protein is sufficient to activate Notch signaling target gene
433 expression (Collu et al., 2012; Wettstein et al., 1997). As *baz* mutations affect the levels of
434 target gene expression and the Baz protein acts genetically at the level of, or in parallel to,
435 NICD, Baz/Par3 might be a factor participating in regulating NICD localization, stability, or
436 modifications to mediate its association with Su(H).
437
438 Interestingly, the human Baz/Par3 homologue, PARD3, has been suggested to act at a similar
439 level in the YAP/TAZ pathway. PARD3, which itself is found in the nucleus in addition to the
440 junction-bound aPKC/Par6 complex, has been suggested to regulate TAZ phosphorylation and
441 its nuclear localization (Zhang et al., 2016), as a scaffold for YAP-binding proteins. The Notch
442 signaling pathway is simpler than the Hippo-YAP/TAZ pathway, as Notch/NICD acts as a
443 "membrane-tethered" transcriptional co-activator, without the complex cascade of kinase-
444 dependent steps as in YAP/TAZ regulation. Nonetheless, NICD is still regulated by
445 phosphorylation events, for example to limit prolonged pathway activity, through the action of
446 Mastermind and CycC:CDK8 (Fryer et al., 2004). It is thus possible that Baz/Par3 may regulate
447 NICD phosphorylation and nuclear localization as well.
448
449 Generally, the strength of activation of target gene expression depends on NICD stability within
450 the resulting activator complexes, which also contain histone modifying/remodeling proteins,
451 and accessibility of enhancers of any given target gene (Borggrefe and Oswald, 2009; Bray,
452 2016). N-signaling acts in many different contexts and can activate many distinct target genes,

453 and as such the presence of context-determining factors will determine whether an enhancer is
454 primed to react to a specific signal, which may result in a gene having different responses
455 towards the same signals (Borggrefe and Oswald, 2009). Our data suggest that Baz/Par3 acts
456 rather generally on NICD mediated target gene activation, as we see effects on Notch target
457 expression in multiple tissues and on different target genes. It is likely that Baz/Par3 is directly
458 or indirectly involved in promoting NICD association with Su(H), and the formation of the Su(H)-
459 NICD-Mam complex. The precise function of Baz/Par3 in the context of NICD regulation will
460 require transcription specific assays to be explored in future studies.
461
462

463 **Materials and Methods**

464 ***Drosophila genetics and strains***

465 *w-IR* ($w^{JF01540}$, P{TRiP.JF01540}), *baz-IR-1* ($baz^{JF01078}$, P{TRiP.JF01078}), *baz-IR-2* ($baz^{JF01079}$,
466 P{TRiP.JF01079}), *aPKC-IR* ($aPKC^{JF01966}$, P{TRiP. JF01966}), *UAS-mCD8RFP,* baz^{4} *FRT9-2*
467 and baz^{815-8} *FRT9-2* fly stocks were obtained from Bloomington Drosophila Stock Center.
468 baz^{815-8} was recombined with FRT19A and then used for baz^{815-8} mutant clonal analysis with
469 FRT19A MARCM stock (genotype: *w, tub-gal80, hs-flp, FRT19A; act-Gal4, UAS-mCD8RFP /*
470 *CyO*). *UAS-numb-GFP* was a gift from Bingwei Lu (Song and Lu, 2012).

471 N^{55e11}/baz^{4} and N^{55e11}/baz^{815-8} were generated by intercrossing via several crosses: *ubi-baz-*
472 *mCherry* (Bosveld et al., 2012) was recombined with Sb^{1} to generate *ubi-baz-mcherry* Sb^{1} flies.
473 baz^{4} (or baz^{815-8}) males with *ubi-baz-mCherry* Sb^{1} which rescued baz^{-} mutations (baz^{4} or baz^{815-}
474 ^{8}; *ubi-baz-mCherry* Sb^{1}/+) were crossed to N^{55e11}/*FM7* females to generate N^{55e11}/baz^{4} or
475 N^{55e11}/baz^{815-8} females (selected against Sb^{1} phenotype).

476

477 *UAS-NICD* (Zaffran and Frasch, 2000) flip-on clones were analyzed and induced together with
478 either *UAS-GFP*, *baz-IR1*, or *baz-IR2*, *UAS-numbGFP*, and *UAS-Su(H)Ank* (full genotypes
479 listed in the figure legends). Third instar larvae were dissected 44-49 hours after clone
480 inductions (which were induced via brief heat-shocks). Control samples from the same set of
481 experiments were heat-shocked, processed and stained together to reduce experimental
482 variations.

483

484 ***DNA constructs:***

485 The *baz*-pENTR was kindly provided by Tony Harris (McKinley et al., 2012). Gateway cloning
486 (Invitrogen) recombined pPWF (from Drosophila Genomics Resource Center) for *UASP-baz* (C-
487 terminal 3X Flag tagged *baz*). The construct was sequenced with *baz* oligos to confirm correct
488 recombination insertion and the Flag tag sequence. Transgenic flies were injected with *UASP-*
489 *baz-Flag* ppWF plasmid by BestGene.

490

491 A fusion of *D. melanogaster* Su(H) and the Notch Ankyrin repeats was designed along the same
492 principle as X-Su(H)-ANK (Wettstein et al., 1997). *Su(H)* coding sequence was cloned from
493 GH10914 (DGRC Stock 5973) into pAc5.1/V5-His A (Invitrogen) using the following primers:
494 Fwd: ACCGGAATTCACCatgaagagctacagccaatt and
495 Rev: ACGCGGATCCggataagccgctaccatgac to remove the stop codon. The sequence encoding
496 Notch Ankyrin repeats were cloned from pAc5.1/N^{IC}-HA (gift of Ram DasGupta) using the
497 following primers:
498 Fwd: ACGCGGATCCgatgtggatgcacgtggacct and
499 Rev: CTTTGCGGCCGCtcacagatcttcttcagaaataagtttttgttcatgctcgtccagcagcctga
500 to introduce a stop codon and myc epitope. The Su(H)-ANK-myc sequence was then subcloned
501 into pUASt-AttB, (and injected into UAS-AttP flies (RRID:BDSC_9724) by BestGene. Multiple
502 transgenic lines were sequenced and phenotypically tested to confirm insertion of the UAS-
503 Su(H)-ANK-myc sequence.
504

505 ***Immunohistochemistry and microscopy:***

506 The following antibodies were used in the study: guinea pig Anti-Baz 1:200 (Blankenship et al.,
507 2007), rabbit anti-Dlg 1:3000-4000 (Izaddoost et al., 2002), mouse anti-Wg 1:10-20 (Brook and
508 Cohen, 1996), mouse Anti-Cut 1:20-1:40 (Blochlinger et al., 1990), rabbit anti-RFP 1:300
509 (Rockland Immunochemicals), rabbit anti-Galactosidase 1:2500 (Cappel). Mouse anti-Cut and
510 anti-Wg antibodies were obtained from Developmental Studies Hybridoma Bank at the
511 University of Iowa.
512

513 Adult wings and nota were imaged with conventional Zeiss Axioplan microscope. Immuno-
514 fluorescent samples were imaged with Leica TCS SP5 or SP8 confocal microscope. Images
515 were projected and quantified with Fiji-Image J. Cut expression levels were measured in cell
516 nuclei marked by Hoechst staining. *baz*$^{815\text{-}8}$ mutant cells were outlined by RFP expression. Only
517 first row of *baz*$^{815\text{-}8}$ mutant cells right at D/V border were measured for “average Cut channel
518 pixel intensity” minus “average background pixel intensity outside Cut expression domain”

519 (similar to Figure S4D1) for each nucleus. Neighboring control A/P border cells were also
520 measured for “average Cut pixel intensity” minus “average background pixel intensity”.
521
522 **Data visualization and Statistics:**
523 Data were plotted via Microsoft Excel, LibreOffice Calc. Fisher’s exact test (two tailed) and
524 student t-test (unpaired) were used for statistical analyses to calculate probabilities of null
525 hypothesis with the web version of Graphpad (Fisher’s exact test) and scipy.stats (t-test).
526
527 **Cell Culture and co-immunoprecipitation**
528 NICD-HA pAc and myc-Hpo pAc were generous gifts from Ramanuj DasGupta and Duojia Pan
529 (Wu et al., 2003). Baz-myc pAWM was generated from pAWM gateway vector (Drosophila
530 Genomics Resource Center) and *baz* pEntr 2B (a gift from Tony Harris).
531 1mg of NICD-HA pAc and Baz-myc pAWM or myc-Hpo pAc plasmids each were transfected
532 into *Drosophila* S2 cells in a 6-well plate with Qiagen Effectene. Cells were lysed one day after
533 transfection with IP buffer (20 mM HEPES pH 7.5, 100 mM NaCl, 0.05% Triton X100, 1 mM
534 EDTA, 5 mM DTT, 10mM NaVO4, 10% glycerol and protease inhibitor cocktail). The cell
535 lysates (1mg of total protein) were pre-cleared by incubating with protein A-sepharose beads
536 (Thermo Scientific 20333) for 1 hour at 4°C, followed by centrifugation to remove the beads.
537 Mouse anti-Myc antibody (sc-40, Santa Cruz technology) was used at 1/1000 dilution for
538 immunoprecipitation. The A-sepharose beads and antibody were incubated together to form
539 pre-immuno-precipitate complexes at 4°C for 1 hour, then incubated with lysates. Myc-tagged
540 protein and associated proteins were captured by protein A-sepharose/antibody complexes after
541 overnight incubation at 4°C. Samples were washed 4 times with IP buffer. Immunoprecipitates
542 were resuspended in SDS sample buffer, boiled for 5 min, separated by SDS-PAGE, and
543 transferred to nitrocellulose membrane for immunoblotting. The blots were incubated with
544 mouse anti-myc (Santa Cruz technology) or rat anti-HA (Roche) at 1:1000, subsequently with

545 anti-mouse or anti-rat IgG-HRP. Proteins were then detected by enhanced chemiluminescence
546 kit (Millipore).
547
548
549
550
551 **Acknowledgements**

552 We are grateful to Kwang-Wook Choi, Kyung-ok Cho, Ramanuj DasGupta, Tony Harris, Duojia
553 Pan, Bingwei Lu, and Jennifer Zallen for *Drosophila* strains and antibodies, and to Cathie
554 Pfleger for helpful suggestions on the manuscript. We also thank the Bloomington Drosophila
555 Stock Center for fly strains, and the Developmental Studies Hybridoma Bank at the University of
556 Iowa for antibodies. We would also like to thank the ISMMS Microscopy CoRE, where confocal
557 microscopy was performed and was in part supported by the Tisch Cancer Institute P30
558 CA196521 grant from the NCI. This work was supported by National Institutes of Health grants
559 R01 EY013256 and R35 GM127103 (to MM).
560
561
562
563 **References:**

564 Andersson, E.R., Sandberg, R., Lendahl, U., 2011. Notch signaling: simplicity in design,
565 versatility in function. Development (Cambridge, England) 138, 3593-3612.

566 Bala Tannan, N., Collu, G., Humphries, A.C., Serysheva, E., Weber, U., Mlodzik, M., 2018.
567 AKAP200 promotes Notch stability by protecting it from Cbl/lysosome-mediated degradation in
568 Drosophila melanogaster. PLoS genetics 14, e1007153.

569 Blankenship, J.T., Fuller, M.T., Zallen, J.A., 2007. The Drosophila homolog of the Exo84
570 exocyst subunit promotes apical epithelial identity. Journal of cell science 120, 3099-3110.

571 Blochlinger, K., Bodmer, R., Jan, L.Y., Jan, Y.N., 1990. Patterns of expression of cut, a protein
572 required for external sensory organ development in wild-type and cut mutant Drosophila
573 embryos. Genes & development 4, 1322-1331.

574 Borggrefe, T., Oswald, F., 2009. The Notch signaling pathway: transcriptional regulation at
575 Notch target genes. Cell Mol Life Sci 66, 1631-1646.

576 Bosveld, F., Bonnet, I., Guirao, B., Tlili, S., Wang, Z., Petitalot, A., Marchand, R., Bardet, P.L.,
577 Marcq, P., Graner, F., Bellaiche, Y., 2012. Mechanical control of morphogenesis by
578 Fat/Dachsous/Four-jointed planar cell polarity pathway. Science (New York, N.Y 336, 724-727.

579 Bray, S.J., 2016. Notch signalling in context. Nat Rev Mol Cell Biol 17, 722-735.

580 Brook, W.J., Cohen, S.M., 1996. Antagonistic interactions between wingless and
581 decapentaplegic responsible for dorsal-ventral pattern in the Drosophila Leg. Science (New
582 York, N.Y 273, 1373-1377.

583 Collu, G.M., Hidalgo-Sastre, A., Acar, A., Bayston, L., Gildea, C., Leverentz, M.K., Mills, C.G.,
584 Owens, T.W., Meurette, O., Dorey, K., Brennan, K., 2012. Dishevelled limits Notch signalling
585 through inhibition of CSL. Development (Cambridge, England) 139, 4405-4415.

586 Cooper, M.T., Bray, S.J., 1999. Frizzled regulation of Notch signalling polarizes cell fate in the
587 Drosophila eye. Nature 397, 526-530.

588 Courbard, J.R., Djiane, A., Wu, J., Mlodzik, M., 2009. The apical/basal-polarity determinant
589 Scribble cooperates with the PCP core factor Stbm/Vang and functions as one of its effectors.
590 Developmental biology 333, 67-77.

591 Couturier, L., Mazouni, K., Schweisguth, F., 2013. Numb localizes at endosomes and controls
592 the endosomal sorting of notch after asymmetric division in Drosophila. Curr Biol 23, 588-593.

593 Djiane, A., Yogev, S., Mlodzik, M., 2005. The apical determinants aPKC and dPatj regulate
594 Frizzled-dependent planar cell polarity in the Drosophila eye. Cell 121, 621-631.

595 Etemad-Moghadam, B., Guo, S., Kemphues, K.J., 1995. Asymmetrically distributed PAR-3
596 protein contributes to cell polarity and spindle alignment in early C. elegans embryos. Cell 83,
597 743-752.

598 Fang, L., Wang, Y., Du, D., Yang, G., Tak Kwok, T., Kai Kong, S., Chen, B., Chen, D.J., Chen,
599 Z., 2007. Cell polarity protein Par3 complexes with DNA-PK via Ku70 and regulates DNA
600 double-strand break repair. Cell research 17, 100-116.

601 Fanto, M., Mlodzik, M., 1999. Asymmetric Notch activation specifies photoreceptors R3 and R4
602 and planar polarity in the Drosophila eye. Nature 397, 523-526.

603 Fleming, R.J., Scottgale, T.N., Diederich, R.J., Artavanis-Tsakonas, S., 1990. The gene Serrate
604 encodes a putative EGF-like transmembrane protein essential for proper ectodermal
605 development in Drosophila melanogaster. Genes & development 4, 2188-2201.

606 Fortini, M.E., Rebay, I., Caron, L.A., Artavanis-Tsakonas, S., 1993. An activated Notch receptor
607 blocks cell-fate commitment in the developing Drosophila eye. Nature 365, 555-557.

608 Freeman, A.B.a.M., 2001. Notch signalling and the initiation of neural development in the
609 Drosophila eye. Development (Cambridge, England) 128, 3889-3898.

610 Frise, E., Knoblich, J.A., Younger-Shepherd, S., Jan, L.Y., Jan, Y.N., 1996. The Drosophila
611 Numb protein inhibits signaling of the Notch receptor during cell-cell interaction in sensory organ
612 lineage. Proceedings of the National Academy of Sciences of the United States of America 93,
613 11925-11932.

614 Fryer, C.J., White, J.B., Jones, K.A., 2004. Mastermind recruits CycC:CDK8 to phosphorylate
615 the Notch ICD and coordinate activation with turnover. Molecular cell 16, 509-520.

616 Furriols, M., Bray, S., 2001. A model Notch response element detects Suppressor of Hairless-
617 dependent molecular switch. Curr Biol 11, 60-64.

618 Goldstein, B., Macara, I.G., 2007. The PAR proteins: fundamental players in animal cell
619 polarization. Developmental cell 13, 609-622.

620 Greenwald, I., 1985. lin-12, a nematode homeotic gene, is homologous to a set of mammalian
621 proteins that includes epidermal growth factor. Cell 43, 583-590.

622 Guo, M., Jan, L.Y., Jan, Y.N., 1996. Control of daughter cell fates during asymmetric division:
623 interaction of Numb and Notch. Neuron 17, 27-41.

624 Guruharsha, K.G., Kankel, M.W., Artavanis-Tsakonas, S., 2012. The Notch signalling system:
625 recent insights into the complexity of a conserved pathway. Nature reviews 13, 654-666.

626 Harris, T.J., Peifer, M., 2004. Adherens junction-dependent and -independent steps in the
627 establishment of epithelial cell polarity in Drosophila. The Journal of cell biology 167, 135-147.

628 Henrique, D., Schweisguth, F., 2019. Mechanisms of Notch signaling: a simple logic deployed in
629 time and space. Development (Cambridge, England) 146, dev172148 doi:
630 172110.171242/dev.172148.

631 Houssin, E., Pinot, M., Bellec, K., Le Borgne, R., 2021. Par3 cooperates with Sanpodo for the
632 assembly of Notch clusters following asymmetric division of Drosophila sensory organ precursor
633 cells. eLife 10.

634 Humphries, A.C., Mlodzik, M., 2018. From instruction to output: Wnt/PCP signaling in
635 development and cancer. Curr Opin Cell Biol 51, 110-116.

636 Izaddoost, S., Nam, S.C., Bhat, M.A., Bellen, H.J., Choi, K.W., 2002. Drosophila Crumbs is a
637 positional cue in photoreceptor adherens junctions and rhabdomeres. Nature 416, 178-183.

638 Jack, J., Dorsett, D., Delotto, Y., Liu, S., 1991. Expression of the cut locus in the Drosophila
639 wing margin is required for cell type specification and is regulated by a distant enhancer.
640 Development (Cambridge, England) 113, 735-747.

641 Kandachar, V., Roegiers, F., 2012. Endocytosis and control of Notch signaling. Curr Opin Cell
642 Biol 24, 534-540.

643 Kassis, J.A., Noll, E., VanSickle, E.P., Odenwald, W.F., Perrimon, N., 1992. Altering the
644 insertional specificity of a Drosophila transposable element. Proceedings of the National
645 Academy of Sciences of the United States of America 89, 1919-1923.

646 Kidd, S., Lieber, T., Young, M.W., 1998. Ligand-induced cleavage and regulation of nuclear
647 entry of Notch in Drosophila melanogaster embryos. Genes & development 12, 3728-3740.

648 Kopan, R., Ilagan, M.X., 2009. The canonical Notch signaling pathway: unfolding the activation
649 mechanism. Cell 137, 216-233.

650 Kopczynski, C.C., Alton, A.K., Fechtel, K., Kooh, P.J., Muskavitch, M.A., 1988. Delta, a
651 Drosophila neurogenic gene, is transcriptionally complex and encodes a protein related to blood
652 coagulation factors and epidermal growth factor of vertebrates. Genes & development 2, 1723-
653 1735.

654 Lindsley, D.L., Zimm, G.G., 1992. The Genome of Drosophila melanogaster.

655 McKinley, R.F., Yu, C.G., Harris, T.J., 2012. Assembly of Bazooka polarity landmarks through a
656 multifaceted membrane-association mechanism. Journal of cell science 125, 1177-1190.

657 Medina-Yáñez, I., Olivares, G.H., Vega-Macaya, F., Mlodzik, M., Olguín, P., 2020. Phosphatidic
658 acid increases Notch signalling by affecting Sanpodo trafficking during Drosophila sensory
659 organ development. Scientific reports 10, 21731.

660 Micchelli, C.A., Rulifson, E.J., Blair, S.S., 1997. The function and regulation of cut expression on
661 the wing margin of Drosophila: Notch, Wingless and a dominant negative role for Delta and
662 Serrate. Development (Cambridge, England) 124, 1485-1495.

663 Mohr, O.L., 1919. Character changes caused by mutation of an entire region of a chromosome
664 in Drosophila. Genetics 4, 275-282.

665 Morais-de-Sa, E., Mirouse, V., St Johnston, D., 2010. aPKC phosphorylation of Bazooka
666 defines the apical/lateral border in Drosophila epithelial cells. Cell 141, 509-523.

667 Muller, H.A., Wieschaus, E., 1996. armadillo, bazooka, and stardust are critical for early stages
668 in formation of the zonula adherens and maintenance of the polarized blastoderm epithelium in
669 Drosophila. The Journal of cell biology 134, 149-163.

670 Neumann, C.J., Cohen, S.M., 1996. A hierarchy of cross-regulation involving Notch, wingless,
671 vestigial and cut organizes the dorsal/ventral axis of the Drosophila wing. Development
672 (Cambridge, England) 122, 3477-3485.

673 Neumuller, R.A., Knoblich, J.A., 2009. Dividing cellular asymmetry: asymmetric cell division and
674 its implications for stem cells and cancer. Genes & development 23, 2675-2699.

675 Rana, N.A., Haltiwanger, R.S., 2011. Fringe benefits: functional and structural impacts of O-
676 glycosylation on the extracellular domain of Notch receptors. Current opinion in structural
677 biology 21, 583-589.

678 Roegiers, F., Younger-Shepherd, S., Jan, L.Y., Jan, Y.N., 2001. Bazooka is required for
679 localization of determinants and controlling proliferation in the sensory organ precursor cell
680 lineage in Drosophila. Proceedings of the National Academy of Sciences of the United States of
681 America 98, 14469-14474.

682 Saj, A., Arziman, Z., Stempfle, D., van Belle, W., Sauder, U., Horn, T., Durrenberger, M., Paro,
683 R., Boutros, M., Merdes, G., 2010. A combined ex vivo and in vivo RNAi screen for notch
684 regulators in Drosophila reveals an extensive notch interaction network. Developmental cell 18,
685 862-876.

686 Schweisguth, F., 2015. Asymmetric cell division in the Drosophila bristle lineage: from the
687 polarization of sensory organ precursor cells to Notch-mediated binary fate decision. Wiley
688 Interdiscip Rev Dev Biol 4, 299-309.

689 Shilo, B.Z., Schejter, E.D., 2011. Regulation of developmental intercellular signalling by
690 intracellular trafficking. Embo j 30, 3516-3526.

691 Siebel, C., Lendahl, U., 2017. Notch Signaling in Development, Tissue Homeostasis, and
692 Disease. Physiol Rev 97, 1235-1294.

693 Singh, J., Mlodzik, M., 2012. Hibris, a Drosophila nephrin homolog, is required for presenilin-
694 mediated Notch and APP-like cleavages. Developmental cell 23, 82-96.

695 Song, Y., Lu, B., 2012. Interaction of Notch signaling modulator Numb with α-Adaptin regulates
696 endocytosis of Notch pathway components and cell fate determination of neural stem cells. The
697 Journal of biological chemistry 287, 17716-17728.

698 Southgate, L., Sukalo, M., Karountzos, A.S.V., Taylor, E.J., Collinson, C.S., Ruddy, D., Snape,
699 K.M., Dallapiccola, B., Tolmie, J.L., Joss, S., Brancati, F., Digilio, M.C., Graul-Neumann, L.M.,
700 Salviati, L., Coerdt, W., Jacquemin, E., Wuyts, W., Zenker, M., Machado, R.D., Trembath, R.C.,
701 2015. Haploinsufficiency of the NOTCH1 Receptor as a Cause of Adams-Oliver Syndrome With
702 Variable Cardiac Anomalies. Circ Cardiovasc Genet 8, 572-581.

703 St Johnston, D., Sanson, B., 2011. Epithelial polarity and morphogenesis. Curr Opin Cell Biol
704 23, 540-546.

705 Struhl, G., Greenwald, I., 1999. Presenilin is required for activity and nuclear access of Notch in
706 Drosophila. Nature 398, 522-525.

707 Suzuki, A., Ohno, S., 2006. The PAR-aPKC system: lessons in polarity. Journal of cell science
708 119, 979-987.

709 Tepass, U., 2012. The apical polarity protein network in Drosophila epithelial cells: regulation of
710 polarity, junctions, morphogenesis, cell growth, and survival. Annual review of cell and
711 developmental biology 28, 655-685.

712 Tomlinson, A., Struhl, G., 1999. Decoding vectorial information from a gradient: sequential roles
713 of the receptors Frizzled and Notch in establishing planar polarity in the Drosophila eye.
714 Development (Cambridge, England) 126, 5725-5738.

715 Tomlinson, A., Struhl, G., 2001. Delta/Notch and Boss/Sevenless signals act combinatorially to
716 specify the Drosophila R7 photoreceptor. Molecular cell 7, 487-495.

717 Weber, U., Eroglu, C., Mlodzik, M., 2003. Phospholipid membrane composition affects EGF
718 receptor and Notch signaling through effects on endocytosis during Drosophila development.
719 Developmental cell 5, 559-570.

720 Wettstein, D.A., Turner, D.L., Kintner, C., 1997. The Xenopus homolog of Drosophila
721 Suppressor of Hairless mediates Notch signaling during primary neurogenesis. Development
722 (Cambridge, England) 124, 693-702.

723 Wharton, K.A., Johansen, K.M., Xu, T., Artavanis-Tsakonas, S., 1985. Nucleotide sequence
724 from the neurogenic locus notch implies a gene product that shares homology with proteins
725 containing EGF-like repeats. Cell 43, 567-581.

726 Wilson, A., Radtke, F., 2006. Multiple functions of Notch signaling in self-renewing organs and
727 cancer. FEBS letters 580, 2860-2868.

728 Wu, S., Huang, J., Dong, J., Pan, D., 2003. hippo encodes a Ste-20 family protein kinase that
729 restricts cell proliferation and promotes apoptosis in conjunction with salvador and warts. Cell
730 114, 445-456.

731 Wu, S., Yang, Y., Tang, R., Zhang, S., Qin, P., Lin, R., Rafel, N., Lucchetta, E.M., Ohlstein, B.,
732 Guo, Z., 2023. Apical-basal polarity precisely determines intestinal stem cell number by
733 regulating Prospero threshold. Cell Rep 42, 112093.

734 Zaffran, S., Frasch, M., 2000. Barbu: an E(spl) m4/m(alpha)-related gene that antagonizes
735 Notch signaling and is required for the establishment of ommatidial polarity. Development
736 (Cambridge, England) 127, 1115-1130.

737 Zhang, P., Wang, S., Wang, S., Qiao, J., Zhang, L., Zhang, Z., Chen, Z., 2016. Dual function of
738 partitioning-defective 3 in the regulation of YAP phosphorylation and activation. Cell Discov 2,
739 16021.

740

741 **Figures**

742 **Figure 1**. Reduction of *bazooka/baz function* causes wing margin bristle loss.

743 (A-D) Overview and high magnification view (A'-D') of wings of the indicated genotypes.

744 (A, A') Wild-type wing; note the associated margin bristles in high magnification of area of

745 posterior wing margin (A'). Cellular hairs point towards the distal margin (green arrow).

746 (B, B') *enGal4, UAS-baz-IR-1* wing, with *baz* knock-down in the posterior compartment; note

747 loss of margin bristles (magenta arrows). Cellular hair orientation was not significantly affected.

748 (Genotype: *UAS-dcr2; enGal4, UAS-RFP, NRE-GFP / UAS-Baz-IR-1 at 29°C*)

749 (C, C') *enGal4, UAS-baz-IR2* wing (independent RNAi, see Fig. S1), displaying similar loss of

750 margin bristles phenotype with hair orientation not significantly affected. (Genotype: *UAS-dcr2;*

751 *enGal4, UAS-RFP, NRE-GFP / UAS-Baz-IR-2 at 29°C*)

752 (D, D') *enGal4, UAS-aPKC-IR* wing, displaying largely normal margin bristle development. Note

753 wing size reduction in posterior compartment with some areas displaying abnormally short wing

754 hairs (orange arrow) and other areas with cellular hair orientation defects, suggesting that

755 reduction of aPKC affected several aspects of wing development, yet had no effect on margin

756 bristle development (Genotype: *enGal4* /+; *UAS-aPKC-IR (aPKC^{JF01966})* /+ at 19°C)

757 (E-E") RNAi-based knock down of Baz protein in posterior compartment. All panels are showing

758 max-projections of a stack of confocal images (~40mm to cover the apical surface of all of the

759 wing pouch area), including composite (E) and individual channels. Anti-Dlg (Discs large, green

760 and E') staining, serves as positive control to outline cells in both anterior (labeled "A") and

761 posterior compartments (labeled "P"). Anti-Baz (magenta) levels were markedly reduced in the

762 posterior *baz-IR* expressing compartment, suggesting an effective knock-down via the *baz* RNAi

763 transgene. (Genotype: *dcr2; enGal4/+; /UAS-baz-IR-2 29°C*).

764

765 **Figure 2.** *Notch* and *baz* interact genetically during wing margin patterning.

766 (A-B) Heterozygous N^{55e11}/+ wings display wing margin notching phenotypes; approx. 2/3 of *N*/+
767 wings are normal with no margin loss (example in A), while 1/3 displayed distal margin notches
768 (B, arrow). Proximal posterior wing margin was always normal (boxed area in B, and B') in all
769 animals. Quantified in panels (F) and (G).
770 (C-D) N^{55e11}/baz^{815-8} double heterozygous wings. Note increased margin notching in distal area
771 (D, arrows) and proximal-posterior wing margin in all wings (C, D and D', arrows). (D') Higher
772 magnification of boxed area in D. Quantified in panels (F) and (G).
773 (E) baz^{815-8}/+ single heterozygous wings show no notching/tissue loss at margin, neither distally
774 nor in the proximal-posterior region (E', boxed area from E shown at higher magnification).
775 (F) Quantification of distal wing margin phenotypes as percentage of wings containing notching
776 (genotypes as indicated). Note that N^{55e11}/baz^{4} and N^{55e11}/baz^{815-8} flies show enhanced defects
777 (higher percentage) of margin notching as compared to N^{55e11}/+ alone (p=0.0062 and p=0.0033,
778 respectively (Fisher's exact test). The control baz^{4}/+ and baz^{815-8}/+ single heterozygous flies
779 have no wing margin phenotypes.
780 (G) Quantification of proximal wing margin phenotypes (posterior compartment) as percentage
781 of wings with margin loss (genotypes as indicated). 100% of N^{55e11}/baz^{4} and N^{55e11}/baz^{815-8} had
782 proximal wing margin notches. N^{55e11}/+, baz^{4}/+ and baz^{815-8}/+ heterozygous flies have no
783 proximal wing margin defects. p<0.0001 (Fisher's exact test) for phenotypic differences between
784 both double heterozygous combinations and N^{55e11}/+.
785 (H) baz^{815-8}/+ heterozygosity suppresses the *sev-NICD*/+ gain-of-function eye phenotype. *sev-*
786 *NICD* induces several phenotypes, and most prominently a transformation of the R1/R6 outer
787 photoreceptors to R7s, which results in ommatidia classified as 4:3 (4 outer R-cells and 3 R7s)
788 or 5:2 (5 outer R-cells and 2 R7s), in contrast to *wt*, which has a 6:1 appearance (6 outer R-cells
789 and 1 R7). Note that heterozygosity of baz suppresses the effect of sev-NICD and reverts the
790 ommatidial appearance partially towards 6:1 (the *wt* appearance).
791

792 **Figure 3.** Notch target gene expression is affected in *baz* mutant cells.

793 (A-C") Confocal images of third instar wing discs with expression of Notch target genes: *wg-lacZ*
794 (detected with anti-bGal, red; monochrome in A', B', and C') and *cut* (anti-Cut, blue;
795 monochrome in A", B", and C") are shown in wild type (A-A"), *baz-IR-1* (B-B"), and *baz-IR-2* (C-
796 C") genotypes. *wg-lacZ* and Cut expression are both reduced within the *enGal4>IR* expression
797 domain (posterior compartment, marked by GFP in green). Genotypes: (A) *UAS-dcr2; enGal4,*
798 *UAS-GFP / wg-lacZ*. (B) *UAS-dcr2; enGal4, UAS-GFP / wg-lacZ; baz-IR-1* (*BL31522)/+*. (C)
799 *UAS-dcr2; enGal4, UAS-GFP / baz-IR-2 (BL31523)/+* (all at 29°C).

800 (D) Quantification of intensity ratio of Cut expression between anterior and posterior
801 compartments (see Materials and Methods for details). Note reduction with both independent
802 *baz-IR* transgenes (*p*-values 0.0003 and 0.0001 (student t-test), respectively). (E) Quantification
803 of intensity ratio of *wg-lacZ* expression (anti-bgal staining) between anterior and posterior
804 compartments (*p*-values 0.002, and 0.001, respectively).

805

806 **Figure 4**. Clones mutant for *baz* display markedly reduced Notch target gene expression in eye
807 and wing discs.

808 (A-A") Confocal optical section of $baz^{815\text{-}8}$ wing disc clone (positively labeled by co-expression of
809 RFP), and (B-B") cross-section of same $baz^{815\text{-}8}$ clone at position indicated by yellow line in (A).
810 Cut expression is reduced in *baz* mutant cells. Yellow line traverses Cut expression domain in
811 two regions indicated by white and blue arrows. Cut levels in $baz^{815\text{-}8}$ mutant cells (white arrow)
812 are reduced, as compared to heterozygous control cells (blue arrows). Genotype: *w, tub-gal80,*
813 *hs-flp, FRT19A/* $baz^{815\text{-}8}$ *FRT19A; act-Gal4, UAS-mCD8RFP /+.* (C-C"') Projection of 3 optical
814 sections at clonal region in D/V border cells, showing Cut (green, monochrome in C"')
815 expressing cells. Cut is normally expressed in two rows, each flanking the D/V-boundary on the
816 respective side. Note that $baz^{815\text{-}8}$ mutant cells (RFP+, in red) in the cells abutting the D/V-
817 boundary express Cut at markedly reduced levels or not at all (examples highlighted by white

818 arrows), nuclei are marked by Hoechst (blue in C, or turquoise in C"). (D) Quantification of Cut
819 expression levels of D/V border cells (measured by average pixel intensity for each cell, see
820 Materials and Methods for details), plotted to compare Cut levels between control and *baz*$^{815\text{-}8}$
821 mutant cells. Note higher Cut expression in neighboring wild-type cells, as compared to *baz*$^{815\text{-}8}$
822 mutant cells.
823 (E-E") Atonal (Ato) expression at and near the morphogenetic furrow (MF) in eye imaginal discs.
824 containing *baz*$^{815\text{-}8}$ mutant clone (marked by absence of GFP expression, red, highlighted by
825 white outlines). Note markedly reduced Ato expression (green) in many mutant cells (orange
826 arrows in E', E"), although some remained unaffected (E' and E", white arrow). All cells,
827 including those with low Ato expression levels, stained equally well with nuclear marker
828 (Hoechst, blue in E, magenta in E'). (F-G") Two z-section views of *baz*$^{815\text{-}8}$ mutant clone in
829 furrow region, with (F) scanned through the middle of Ato expression stripe. Note that many
830 *baz*$^{815\text{-}8}$ mutant cells displayed markedly reduced or lost Ato expression (orange arrows in F")
831 with Hoechst (Hoechst, blue in F,G and magenta in F',G') staining serving as control. (G) z-
832 scan through posterior region of Ato expression stripe, where scan-plane intersected with the
833 apical domain (due to tissue shape of the MF and pseudo-stratified epithelium of imaginal disc)
834 reflecting junctional marker Patj (blue in G, magenta in G"). Note that apical junctional region
835 remains intact in *baz*$^{815\text{-}8}$ mutant cells, indicating that apical-basal polarity was not affected.
836 Genotype: *baz*$^{815\text{-}8}$ *FRT9-2/hsflp ubi-GFP FRT9-2*. (H) Quantification of Ato expressing cells in
837 *baz*$^{815\text{-}}$ clones and neighboring wild-type control cells revealed a decrease in Ato positive cells in
838 *baz*$^{815\text{-}}$ mutant clone vs wild-type control. Distributions were significantly different based on
839 Fisher's exact test.
840
841 **Figure 5.** Baz acts at the level of NICD or further downstream within Notch signaling.
842 (A-A') NDECD expressed via flip-out clones induces ectopic Wg expression within wing blade
843 precursor cells (Wg in red, monochrome in A'; clones labeled by co-expression of GFP in A).

844 Endogenous Wg expression stripe at DV-boundary serves as control (blue arrow in A') here and
845 in other genotypes, clones overlapping with endogenous Wg stripe were not scored in
846 quantification. Arrowheads mark examples of NDECD expressing clones (white in A, red in A'),
847 many of which induce Wg expression. Only clones in the wing pouch proper (pouch outlined by
848 green lines) were scored for Wg expression. Genotype: *hsflp/UAS-dcr2; act>y*$^{+}$*>Gal4, UAS-*
849 *GFP/+; UAS-NDECD /+.*
850 (B-B') Clonal co-expression of NDECD with *baz-IR-2* markedly reduced the number of Wg
851 expressing clones (Wg in red, monochrome in B'; clones labeled by co-expression of GFP).
852 Arrowheads mark examples of NDECD expressing clones (white in B, red in B'); note reduction
853 in such clones expressing Wg (compare to A,A') Genotype: *hsflp/ UAS-dcr2; act5c>y*$^{+}$*>Gal4,*
854 *UAS-GFP/+; UAS-NDECD /baz-IR-2*.
855 (C-C') NICD expressing clones induce ectopic Wg expression with high frequency (Wg in red,
856 monochrome in C'; clones labeled by GFP). Arrowheads highlight examples of NICD expressing
857 clones (white in C, red in C'). Genotype: *hsflp/UAS-dcr2: act5c>y*$^{+}$*>Gal4, UAS-GFP/+; UAS-*
858 *NICD /+.*
859 (D-D') *IR* control (*white*/*w-IR*) co-expressed in NICD in clones. Ectopic Wg expression was
860 induced at similar frequencies to NICD alone (Wg in red, monochrome in D'; clones labeled by
861 GFP). Arrowheads highlight examples of NICD expressing clones (white in D, red in D').
862 Genotype: *hsflp/UAS-dcr2: act5c>y*$^{+}$*>Gal4, UAS-GFP/ UAS-NICD /*+; *w-IR/*+.
863 (E-E') Clonal co-expression of NICD with *baz-IR-2* markedly reduced the number of Wg
864 expressing clones (Wg in red, monochrome in E'; clones labeled by GFP). Arrowheads highlight
865 examples of NICD expressing clones (white in E, red in E'). Genotype: *hsflp/ UAS-dcr2;*
866 *act5c>y*$^{+}$*>Gal4, UAS-GFP/UAS-NICD; baz-IR-2/+.*
867 (F) Quantification of NDECD clones with induced Wg expression with or without *baz-IR(s)*. The
868 frequency of Wg activation in *>NDECD* clones was markedly reduced by the presence of *baz-*

869 *IR-1 or baz-IR-2* (*p*=0.0008 or *p*=0.011, respectively). Only clones inside wing pouch region
870 were counted, due to *wg* expression being regulated by other pathways outside pouch region.
871 (G) Quantification of NICD expressing clones with induced Wg expression with genotypes as
872 indicated (with *w-IR* (control), *baz-IR-1*, and *baz-IR-2*). Wg expression frequency in NICD clones
873 was markedly reduced when *baz-IR-1 or baz-IR-2* were co-expressed (both *p*<0.001 comparing
874 to NICD alone or NICD with *w-IR*; as calculated by Fisher's exact test).
875
876 **Figure 6.** Baz is detected in the same protein complex as NICD.
877 Baz (myc-tagged) or myc-Hippo (Hpo, negative control) and HA-tagged NICD were co-
878 transfected into S2 cells. Lysates of transfected cells were immnunoprecipitated (IP-ed) with
879 anti-myc antibody.
880 (A) Upper panel: Western blot showing NICD-HA detected in lysates of cells co-transfected with
881 myc-Hpo or Baz-myc. Lower panel: Anti-myc co-IP experiments, note NICD-HA was co-IPed
882 with Baz-myc, whereas it was not IP-ed by myc-Hpo (specificity control).
883 (B) Both Baz-myc and myc-Hpo were efficiently pulled down with anti-Myc in cell lysates co-
884 transfected with NICD-HA.
885
886 **Figure 7**. *baz* and *numb* act antagonistically to each other, but at different levels within the
887 Notch pathway
888 (A-F) Wings expressing *baz RNAi* in the posterior compartment in wild-type (*baz-IR-1* in A,A'
889 and *baz-IR-2* in D,D') causing wing margin bristle cell loss (also compare to Figure 1) or the
890 equivalent *baz-IRs* in a *numb* heterozygous background, $numb^{15}$/+ (in B,B' and E,E',
891 respectively). Quantifications, as bristle number, in (C) and (F); wild-type posterior wing margin
892 has on average 230 bristle cells (Suppl. Figure S6). Note that removing a copy of *numb*
893 suppresses the effect of either *baz-RNAi*. Experiments were carried out at 29°C. Genotypes: (A,
894 A') *UAS-dcr2/+; enGal4/+; baz-IR-1/+*. (B,B') *UAS-dcr2/+; enGal4/*$numb^{15}$*; baz-IR-1/+, .* (D,D')

895 *UAS-dcr2/+; enGal4/+; baz-IR-2/+*. (E,E'') *UAS-dcr2/+; enGal4/ numb^{15}; baz-IR-2/+,*. Note that
896 *baz-IR-2* causes stronger defects, and that the phenotypic suppression caused by *numb^{15}*
897 *heterozygosity* was significant (t-test) in both cases (C and F, respectively). "n" = number of
898 wings analyzed. A', B', D', and E' show higher magnification of the corresponding wings shown.
899 (G-I) Induction of Notch target gene expression by NICD expressing clones was not affected by
900 Numb co-overexpression. NICD was expressed via flip-on clones, as in Figure 5, with clones
901 labeled with GFP or numb-GFP co-expression. (G) Confocal optical projection with NICD and
902 GFP expressing clones (control). Note ectopic induction of the Notch target gene *cut*, visualized
903 via anti-Cut immunohistochemical staining (red and monochrome in G'), in many NICD clones.
904 Cut is normally expressed in a stripe at the dorsal/ventral boundary (arrow, in panel G).
905 Genotype: *hsFlp/+; act5c>y>Gal4, UAS-GFP/UAS-NICD*. (H) Projection of wing disc confocal
906 optical sections containing NICD expressing clones (marked in green by Numb-GFP co-
907 expression) with Numb-GFP overexpressed together with NICD. Note ectopic induction of *cut*
908 expression in many clones within the wing pouch. Genotype: *hsFlp/+; act5c>y>Gal4, UAS-*
909 *numb-GFP/UAS-NICD*. (I) Quantification of the percent of Cut expression positive clones in
910 NICD/GFP and NICD/numb-GFP expressing clones. Note similar ratio of expressing clones in
911 both genotypes with no significant difference (p = 0.702 based on Fisher's exact test; "n"
912 indicates the number of clones).
913

914 **Figure 1:**

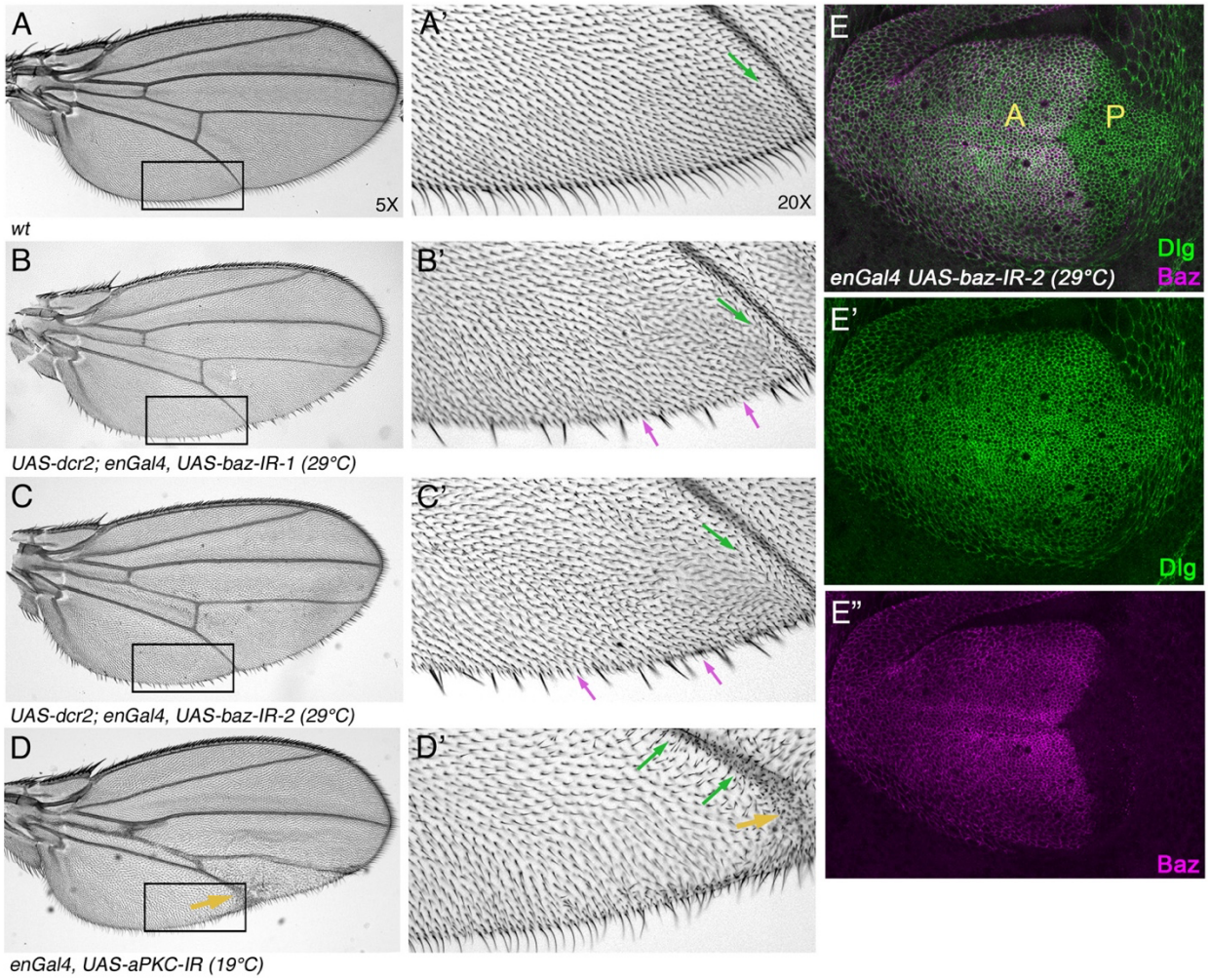

915

916

917 **Figure 2:**

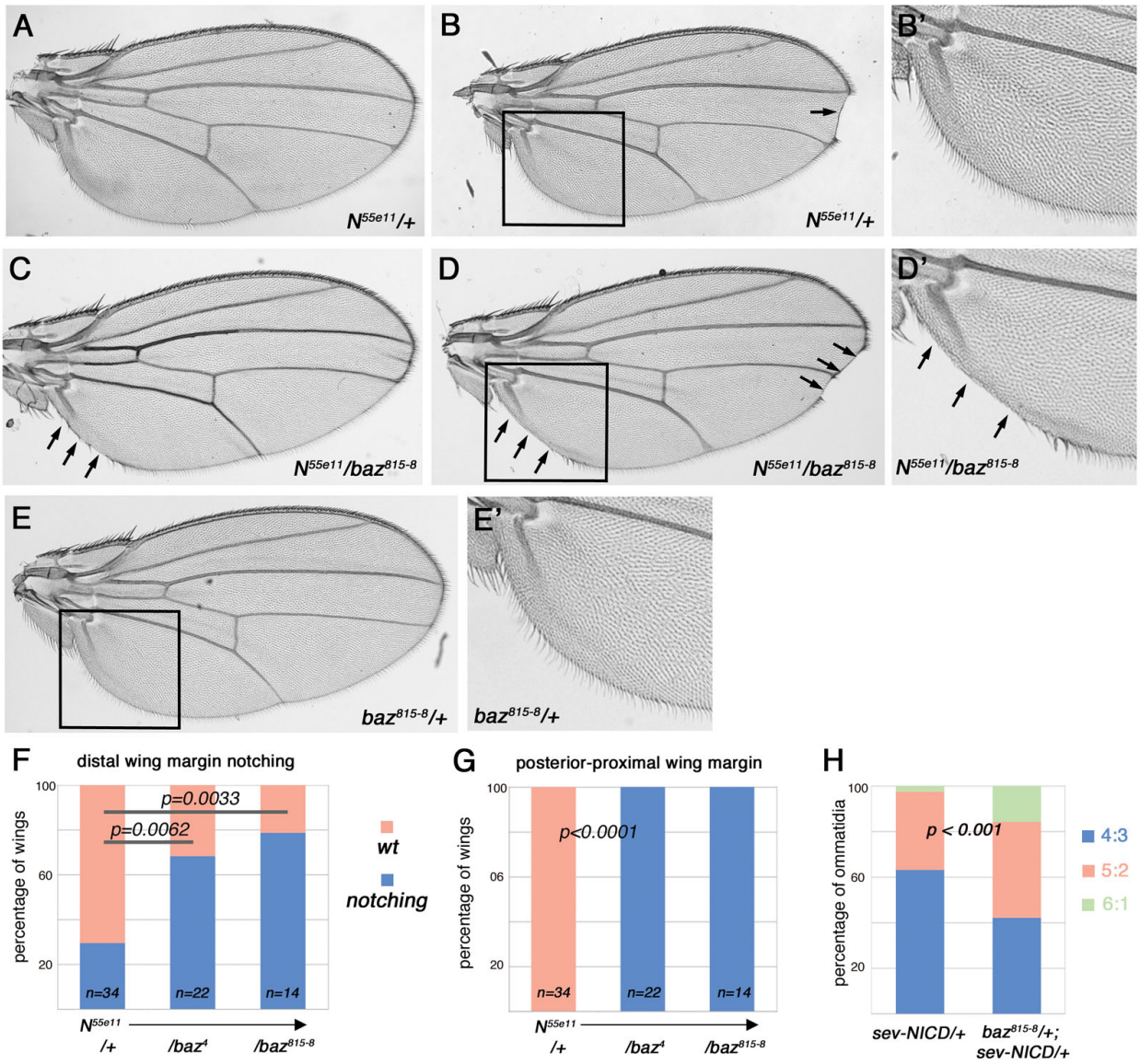

918

919

920

921 **Figure 3:**

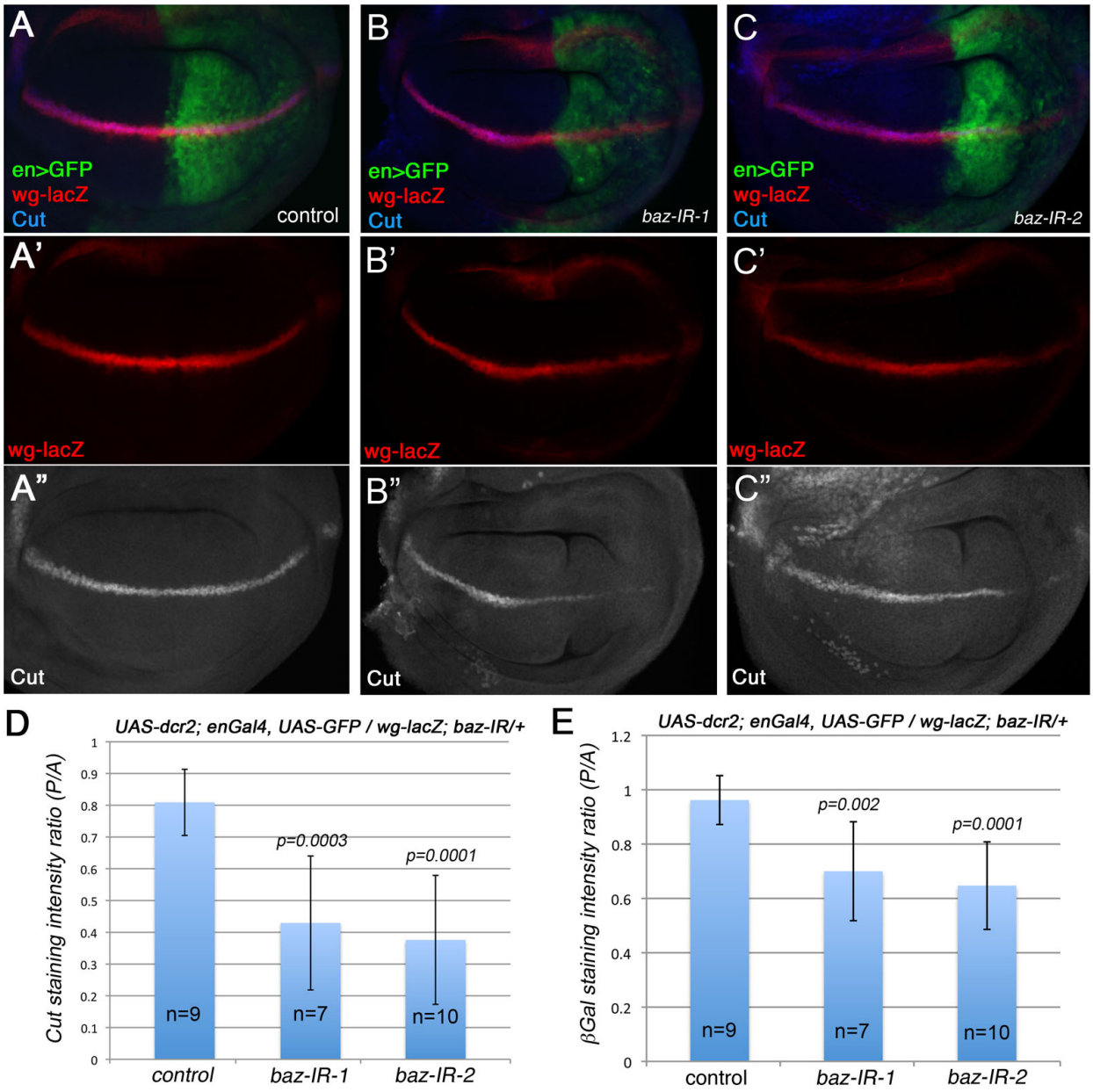

922

923

Figure 4:

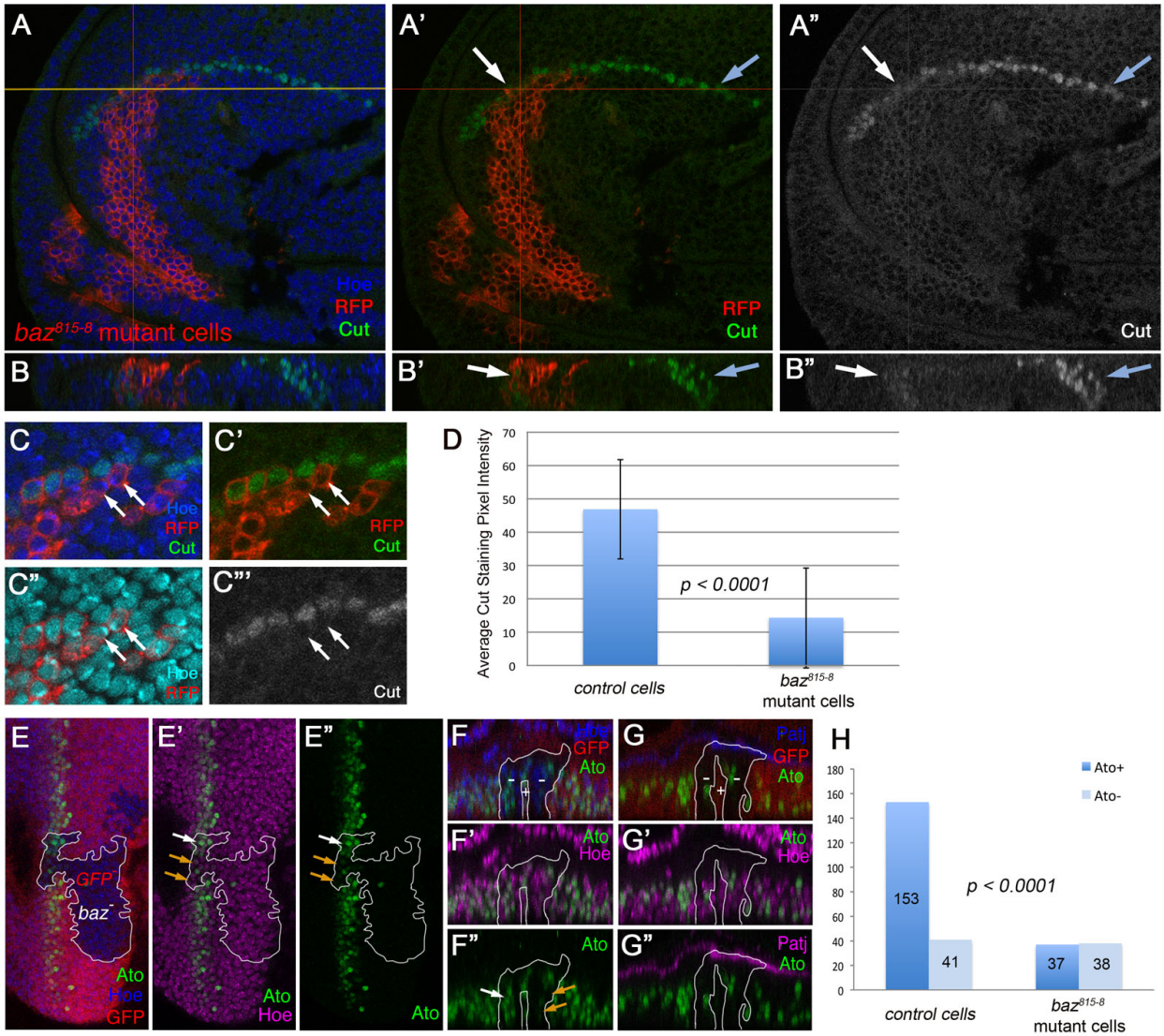
A
Hoe
RFP
Cut
baz815-8 mutant cells
A'
RFP
Cut
A"
Cut
B
B'
B"
C
Hoe
RFP
Cut
C'
RFP
Cut
C"
Hoe
RFP
C'''
Cut
D
Average Cut Staining Pixel Intensity
70
60
50
40
30
20
10
0
p < 0.0001
control cells
baz815-8
mutant cells
E
GFP
baz-
Ato
Hoe
GFP
E'
Ato
Hoe
E"
Ato
F
Hoe
GFP
Ato
F'
Ato
Hoe
F"
Ato
G
Patj
GFP
Ato
G'
Ato
Hoe
G"
Patj
Ato
H
Ato+
Ato-
180
160
140
120
100
80
60
40
20
0
153
41
37
38
p < 0.0001
control cells
baz815-8
mutant cells

927 **Figure 5:**

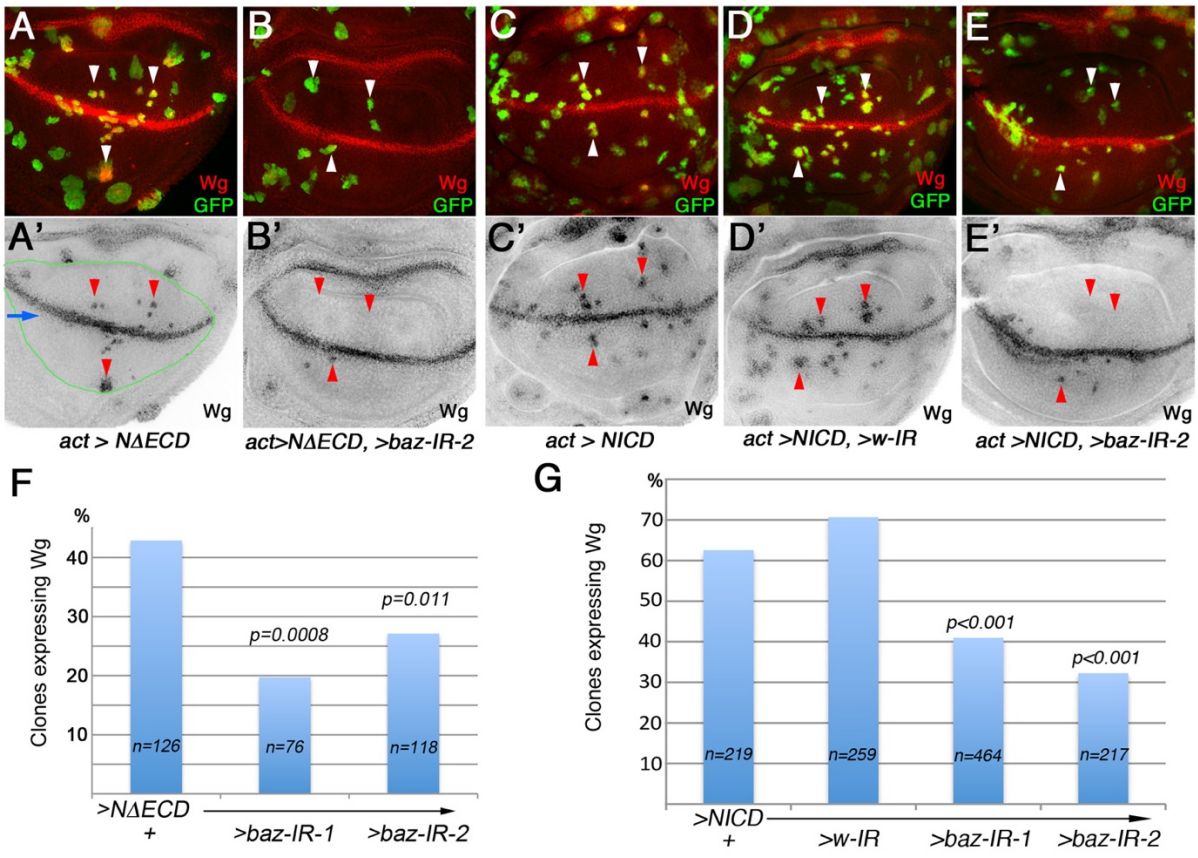

928

929

930 **Figure 6:**

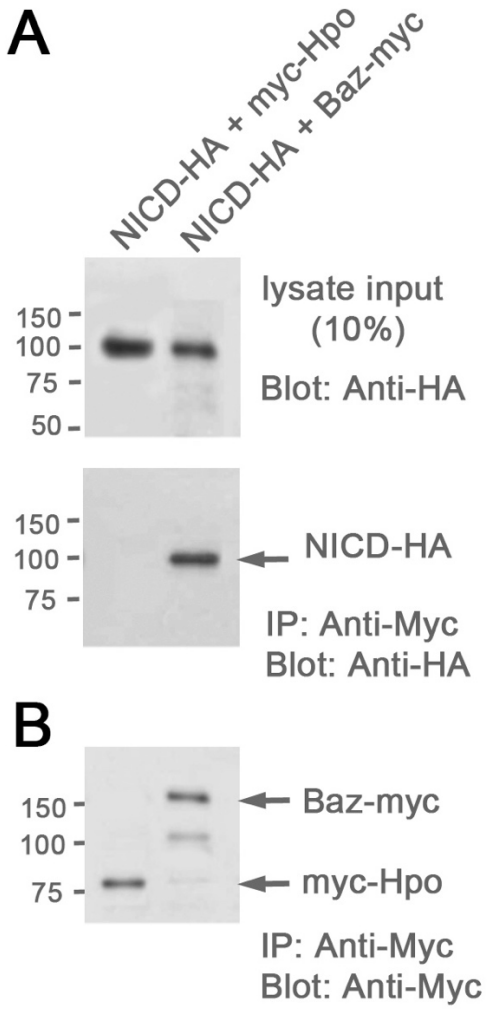

931

932

933 **Figure 7:**

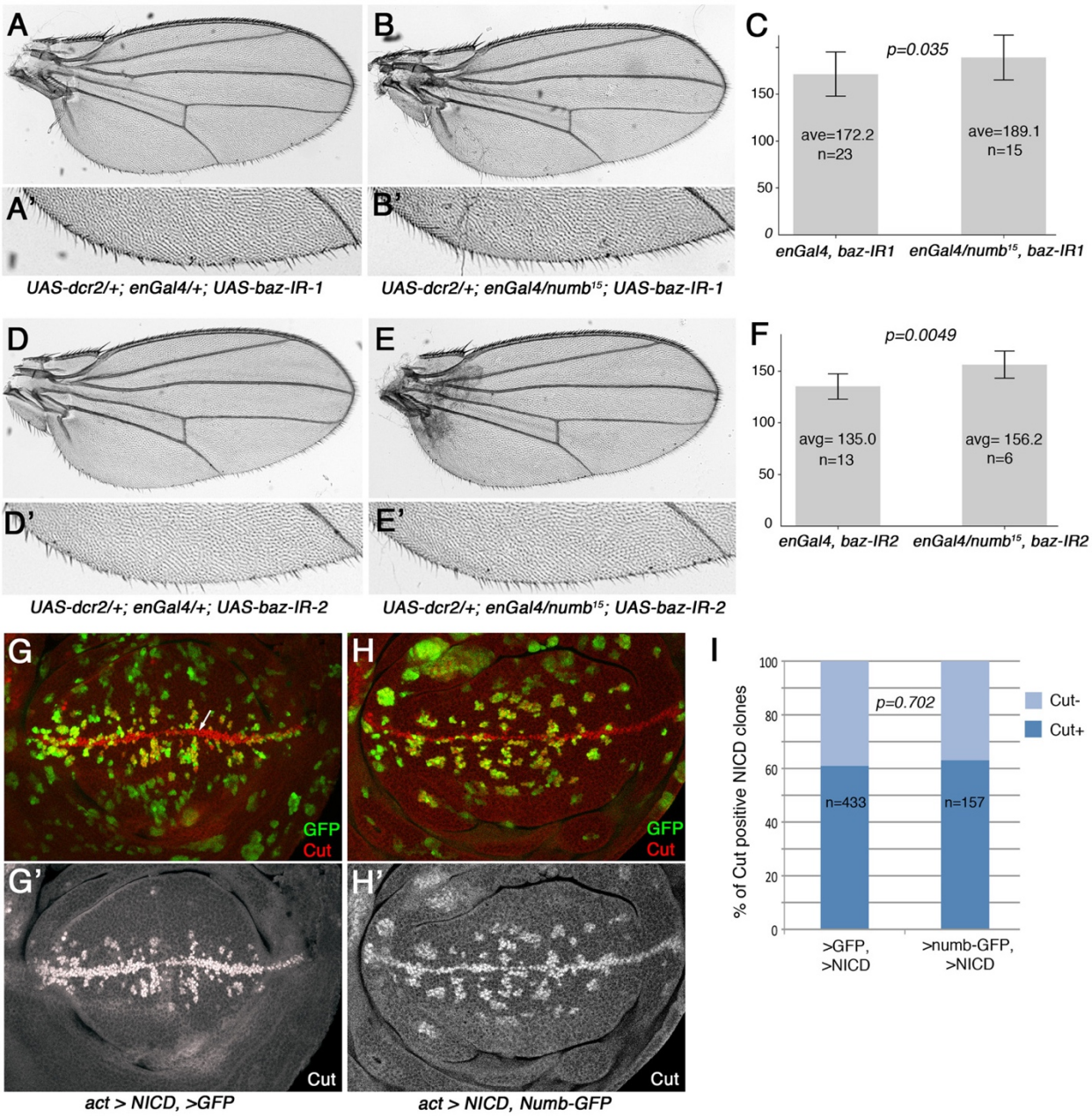

934

935